Effect of Core Diameter, Surface Coating, and PEG Chain Length on the Biodistribution of Persistent Luminescence Nanoparticles in Mice

Thomas Maldiney,* Cyrille Richard,* Johanne Seguin, Nicolas Wattier, Michel Bessodes, and Daniel Scherman

Unité de Pharmacologie Chimique et Génétique et d'Imagerie, CNRS, UMR 8151, Paris, F-75270 cedex France, Inserm, U1022, Paris, F-75270 cedex France, Université Paris Descartes, Faculté des Sciences Pharmaceutiques et Biologiques, Paris, F-75270 cedex France, ENSCP, Paris, F-75231 cedex France, Chimie Paristech, France

ABSTRACT A growing insight toward optical sensors has led to several major improvements in the development of convenient probes for *in vivo* imaging. Efficient optical detection using quantum dots (QDs) as well as near-infrared organic dyes relies on several key driving principles: the ability to lower background absorption or autofluorescence from tissue, a good photostability of the probe, and a high quantum yield. In this article, we report the real-time biodistribution monitoring of lanthanide-doped persistent luminescence nanoparticles (PLNP), emitting in the near-infrared window, in healthy and tumor-bearing mice. We focused on the influence of hydrodynamic diameter, ranging from 80 to 180 nm, and polyethylene glycol (PEG) surface coating on the behavior of our probes. Tissue distribution was found to be highly dependent on surface coverage as well as core diameter. The amount of PLNP in the blood was highly increased for small ($d < 80$ nm) and stealth particles. On the opposite, PEG shield molecular weight, ranging from 5 to 20 kDa, had only negligible influence on the *in vivo* biodistribution of our silicate-based material.

KEYWORDS: nanoparticle · luminescence · biodistribution · PEGylation · tumor targeting · 3LL

By using fluorescent organic dyes to luminescent nanocrystals, optical imaging raises growing interest for the understanding of physiological mechanisms or new diagnosis and therapeutic applications.[1] Photonic probes offer not only practicable living sensors, but also rely on low-cost or affordable imaging devices and techniques. The semiconductor quantum dots[2,3] exhibit high quantum yield, good photostability, and tunable emission wavelength. Luminescent porous silicon nanoparticles can act as both diagnostic[4] and therapeutic tool.[5] At last, near-infrared fluorescent molecules,[6] show some ability to overcome the autofluorescence from tissues under constant illumination.

Each of the above quoted probes displays characteristics that limit future therapeutic application. First, the emission wavelength of semiconductor QDs must be tuned by changing the particle diameter (ranging from 2 to 10 nm) or the composition. On the one hand, this opens alternatives for renal clearance,[7] but it also shortens circulation time of the probe and impairs effective targeting, levying strict regulations on its design.[8] Luminescent porous silicon nanoparticles show great promise as nontoxic, self-destructive, and traceable cargo for anticancer drugs, but they suffer from limited quantum yield[9] (~10%) compared to QDs (>80% in organic solvent). As for near-infrared fluorescent probes, it is now well established that organic dyes are susceptible to photobleaching and are most often unstable under physiological conditions, which make them hardly the best candidate for a long-term biological or biomedical purpose.[10]

We previously reported the synthesis of an inorganic optical nanoprobe ($Ca_{0.2}Zn_{0.9}Mg_{0.9}Si_2O_6$) doped with rare-earth cations (Eu^{2+}, Dy^{3+}, Mn^{2+}), which possesses near-infrared persistent luminescence.[11] Mimicking a capacitor, this material can be excited under UV light a few minutes before use and subsequently emits in the near-infrared window for about 1 h without the need for further illumination. This material could be used to monitor real-time biodistribution in mice,[12] but it displayed major uptake by reticulo-endothelial system (RES) organs (mostly liver and spleen), even after surface functionalization with 5 kDa PEG polymers.

Starting from the recent observation that increasing PEG chain length could slow down RES uptake,[13] we have presently studied the effect of methoxy-PEG coating of different molecular weights (5, 10, and 20 kDa) on the biodistribution of PLNP of various sizes in healthy and tumor-bearing mice.

RESULTS AND DISCUSSION

PLNP Characterization. Starting from hydroxyl-PLNP, polyethylene glycol coating of our

* Address correspondence to cyrille.richard@parisdescartes.fr, thomas.maldiney@parisdescartes.fr.

Received for review August 6, 2010 and accepted January 25, 2011.

Published online February 03, 2011
10.1021/nn101937h

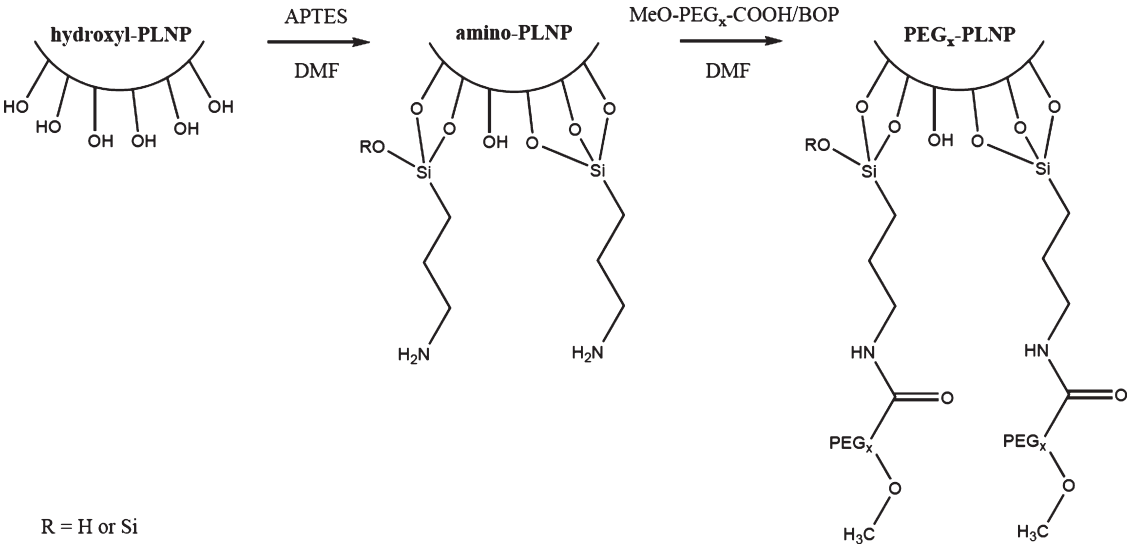

Scheme 1. Schematic representation of amino-PLNP and PEG-PLNP synthesis from the unconjugated hydroxyl-PLNP (*x* referring to PEG molecular weight, being 5000, 10000, or 20000 Da).

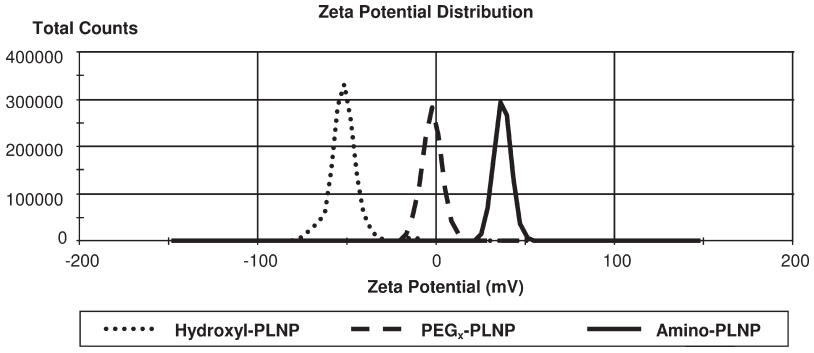

Figure 1. Zeta potential distribution in 20 mM NaCl for differently coated nanoparticles.

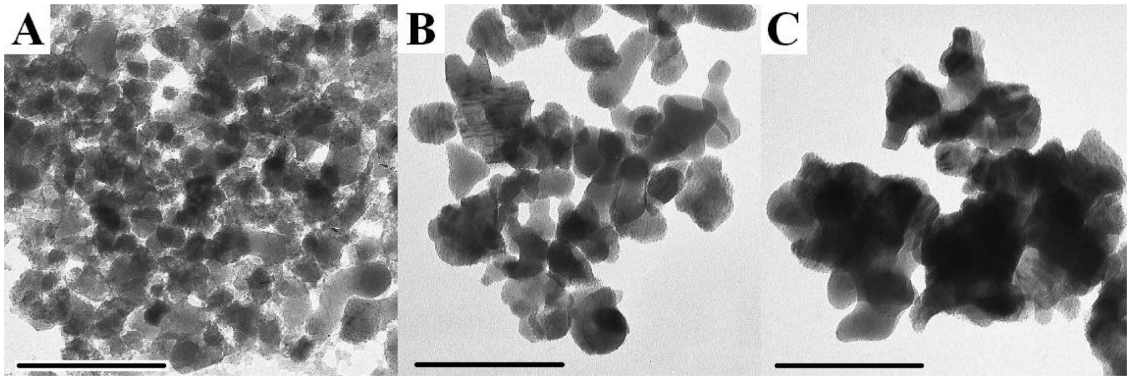

Figure 2. TEM of hydroxyl-PLNP suspended in water: 80 nm (A), 120 nm (B), and 180 nm (C). Scale bar represents 100 nm.

silicate-based nanoparticles was achieved through the formation of amino-PLNP (Scheme 1). Hydrodynamic diameter and zeta potential were monitored to follow the functionalization. Prior to any modification of the surface, hydroxyl groups are responsible for a global negative zeta potential (−50 mV) of the core particle (Figure 1). After aminosilanization, all intermediates were characterized by a straight positive zeta potential ranging from +35 to +40 mV corresponding to the amino-terminated silanes covering the probe (Figure 1). Once the PEG layer coated the nanoparticle, zeta potential switched from positive to neutral values, no matter how long the chain length or wide the particle (Figure 1).

Table S1 (in Supporting Information) displays the hydrodynamic diameter in water before any surface modification and after PEG grafting. First, selective sedimentation allowed us to isolate three different populations from the initial polydisperse colloidal solution, approximately centered on 80, 120, and 180 nm. TEM of

hydroxyl-PLNP suspended in water for all three populations are shown in Figure 2. We notice a significant shift from core diameter obtained by transmission electron micrographs and DLS measurements. This gap was highly predictable, since DLS measurements uses Brownian movement of the solvated particle, it assumes that the particle is spherical in shape and covered with a solvent layer, whereas in the case of TEM, the solvent cannot be seen and we distinguish that bare PLNP are not exact spheroids. The addition of polyethylene glycol significantly changes the average value of hydrodynamic diameter, leading to particles from 40 to 70 nm larger than the initial hydroxyl-PLNP and providing high colloidal stability in normal saline solution, as shown in Figure 3. The PEG coverage is certainly not the only reason that explains such a wide increase in the particle diameter. Indeed, it has been observed that the aminosilanes used in the first functionalization step are likely to form a layer on the particle whose thickness can be up to 10 nm.[14] As shown in Supporting Information Table S1 and contrary to an already assumed trend for a core-diameter to expand with the polymer chain on its surface,[15] in the case of our silicate-based nanoparticles, PEG length does not seem to have much impact on the overall hydrodynamic diameter. This tendency, which has already been observed for poly methoxypolyethyleneglycol cyanoacrylate-co-*n*-hexadecyl cyanoacrylate (PEG-PHDCA) nanoparticles[16] with sizes approximately ranging from 80 to 250 nm, may be because larger PEG chain lengths attach to a lesser extent on the surface of PLNP, then limit the size effect of longer PEG, or to the relatively big size of the core, masking the effect of polymer extension.

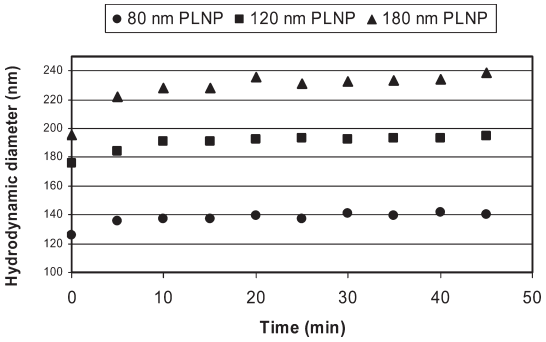

Figure 3. Colloidal stability of 5 kDa PEG-PLNP: evolution of the hydrodynamic diameter in 150 mM NaCl for 45 min.

To further characterize surface properties of our probes, weight loss curves for 120 nm PLNP were obtained from thermogravimetric analysis (TGA) after each functionalization step (Figure 4). From amino-PLNP to PEGylated PLNP we clearly distinguish two stages in surface decomposition. First, water trapped in the organic layer on the surface of PLNP evaporates before 325 °C. The second stage begins after 325 °C and corresponds to the decomposition of organic APTES and PEG coverage on the particles. When comparing TG curves for different PEG, we notice that the longer the PEG chain length, the fewer PEGylated chains remain grafted on the surface. Calculated values from weight loss percentages indicate that in the case of 5 kDa PEG, polymer concentration reaches about 15 nmol/mg of PLNP. This value drops significantly when increasing the size of the PEG to 9 nmol/mg for 10 kDa PEG and 3 nmol/mg for 20 kDa PEG. Despite the 20-fold molar excess of PEG (compared to the amount of free amino groups previously estimated on the surface: about 60 nmol/mg), it seems that steric hindrance hampers the approach of larger PEG near the particle, thus preventing quantitative reaction as well as equimolar loadings of the different PEG.

In a previous work, we have demonstrated that particle functionalization has only a negligible effect on the persistent luminescence properties (data not shown). As the same mass was to be injected for each

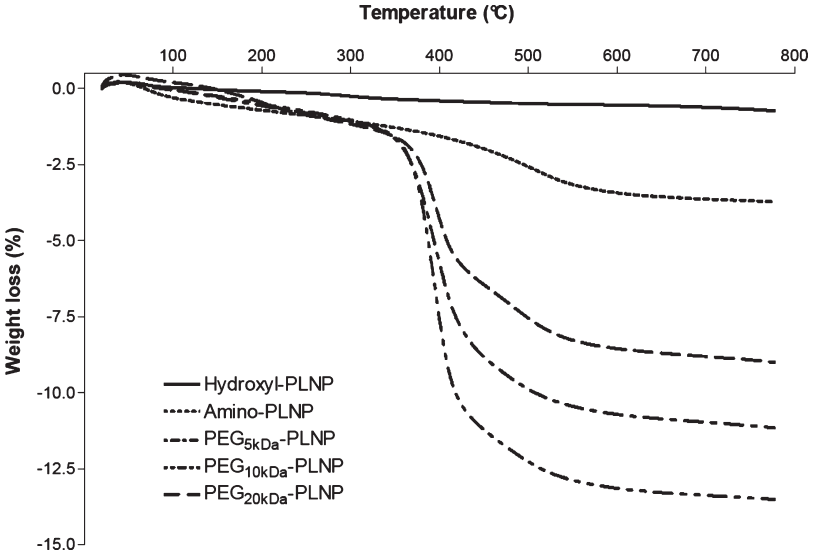

Figure 4. Weight loss curves for 120 nm PLNP with different surface coverage.

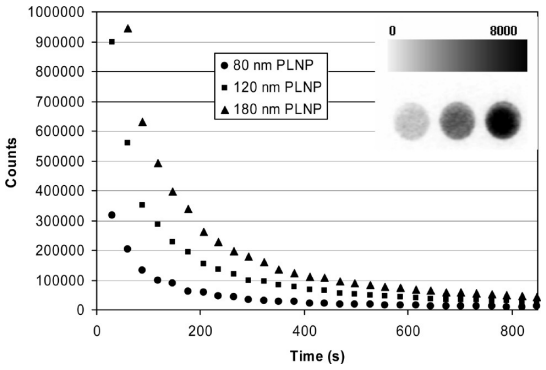

Figure 5. Luminescence decline curve of hydroxyl-PLNP in water (2 mg). The insert represents the corresponding image obtained after a 15 min acquisition (from left to right: 80, 120, and 180 nm hydroxyl-PLNP; luminescence intensity is expressed in gray unit: 1 unit = 2800 photons per s cm^2 steradians).

size population, we wanted to compare their luminescence properties under the photon-counting system. Figure 5 shows the influence of diameter on the emission behavior of hydroxyl-PLNP during the first 13 min after excitation. Luminescence intensity decreases with the diameter of the particle: 180 nm crystals were approximately 5 times brighter than 80 nm ones. To date, the mechanism of persistent luminescence has not yet been elucidated, and the major driving forces responsible for this phenomenon remain unclear.[17] Among the many processes discussed in literature, incorporated defects[18] in the structure (typically holes and electrons), or surface[19] properties, seem to have a major impact on the final optical signature of the crystal. In the case of our silicate-based nanoparticles, the loss of luminescence energy associated with smaller cores could be either due to a decreased probability to find all three doping cations in an infinitesimal volume element (volume effect), or to a variation in the surface to volume ratio, which can be related to nonradiative recombination and quenching.[20] However, the emission lifetime was equivalent for all populations.

Imaging Study and Semiquantitative Biodistribution in RES. PLNP biodistribution is dramatically dependent on surface functionalization (Figure 6). Within a few minutes only, 120 nm hydroxyl-PLNP appear to be quickly trapped in the liver. Indeed, the main lower and pectoral limbs' circulation routes remain hardly distinguishable. Adding the PEG coverage leads to an improved PLNP systemic distribution and to the lighting of the most vascularized areas, such as lower limb and liver which permanently shelters about 10% of the total blood. For larger particles, of 180 nm core diameter, PEG coverage seemed to lead to spleen accumulation (Figure 6). These observations highly corroborate the results from our first imaging study with carboxyl-PLNP and 5 kDa PEG-PLNP, emphasizing the critical role of surface charge in PLNP distribution. Owing to the global negative charge of their hydroxyl groups under physiological conditions in mice (pH = 7.4), hydroxyl-PLNP happened to be quickly localized within liver, subjected to the same recognition process than carboxyl-PLNP with Kupffer cells in liver. Neutral PLNP, acquired through PEGylation, hamper interaction with opsonins and circumvent uptake process. This selectivity for negatively charged nanoparticles toward liver was also observed with organically modified silica (ORMOSIL) nanoparticles. In a recent study combining PET and fluorescence imaging, Kumar *et al.* proved that interaction with serum proteins was favored for nanoparticles displaying a global negative surface charge, leading to larger particle−protein systems (more likely to undergo the uptake process). A great majority of dye (DY776) conjugated ORMOSIL nanoparticles thus quickly accumulated in liver.[21]

Since liver and spleen are blood reservoirs, it can be hard to visually dissociate the amount of free PLNP in the blood circulation from the PLNP trapped in Kupffer cells or splenic macrophages. Therefore, in order to precise the short-term PLNP biodistribution, we focused on two well-defined regions of interest (ROI), comprising liver (Figure 6, left) and spleen (Figure 6, right), and compared the luminescence emitted from these ROI to the global luminescence signal arising from the mouse. The use of our biospace photon-counting process (Photon-Imager) led to an optical semiquantization of the amount of PLNP localized in the liver and spleen 15 min after the injection. Given the little difference observed between 5, 10, and 20 kDa PEG-covered nanoparticles (data not shown), an average value was calculated from all three PEG chain lengths. Figure 7 reports the percentage of total luminescence retained within these two major RES organs for hydroxyl-PLNP and PEG-grafted PLNP.

As shown in Figure 7A, crude material predominantly ends in the liver. Indeed, 15 min after the injection of negatively charged 180 nm particles, almost 70% of the total intensity is located in the liver. This percentage decreases with the diameter and finally reaches the value of approximately 25% for 80 nm hydroxyl-PLNP. As larger particles are almost instantly trapped in the liver, they do not have enough time to circulate through the other organs (spleen, in particular). On the contrary, small particles run longer through the vascular network gaining time to come across splenic macrophages. This is probably the reason why we observe, yet less intense, an opposite trend for hydroxyl-PLNP in the spleen (Figure 7B).

PEG-coated nanoparticles globally distributed much better through the organism. Indeed, with 180 nm PEG-PLNP, only 23% of total luminescence was observed in liver after 15 min (compared to 70% with hydroxyl-PLNP). For 80 nm PEG-PLNP, this proportion falls down to 14%, which represents almost the same value as the percentage of blood constantly running through the organ. Ballou *et al.* witnessed the same effect with PEGylated covered QDs and showed that methoxy-terminated 5 kDa PEG could slowed down the uptake process in

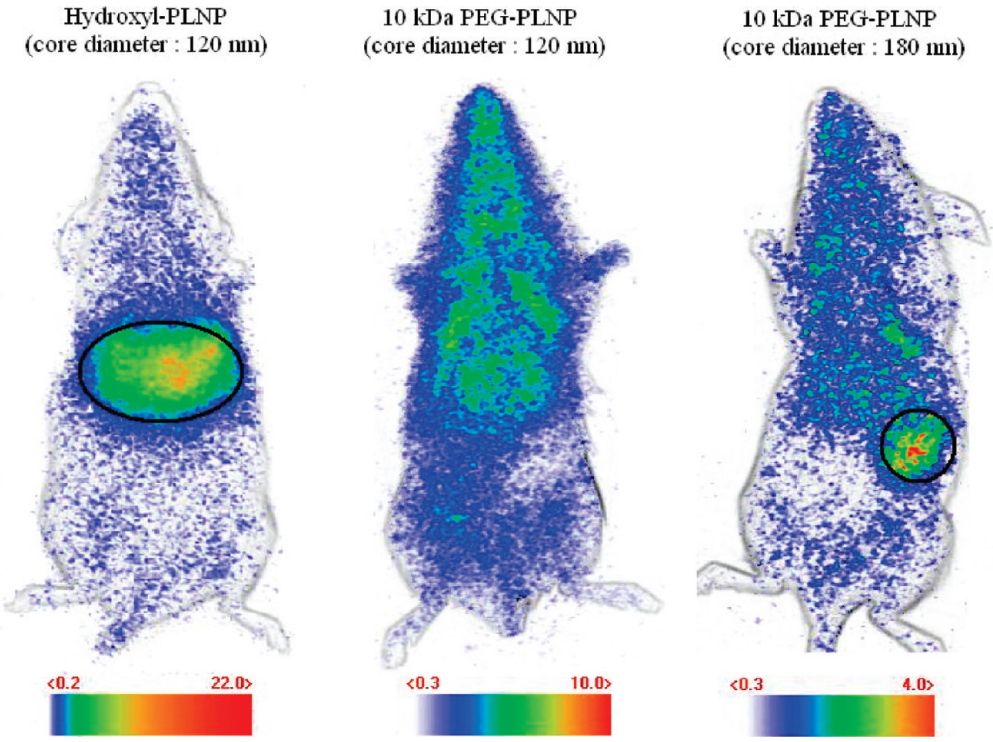

Figure 6. *In vivo* **imaging of different PLNP under the photon-counting system. The signal was acquired for 15 min following systemic injection of the probes (300 μg). Luminescence intensity is expressed in false color unit (1 unit = 2800 photons per s.cm^2. steradians). Dark lines represent drawn ROI for the optical semiquantization (liver on the left image; spleen on the right image).**

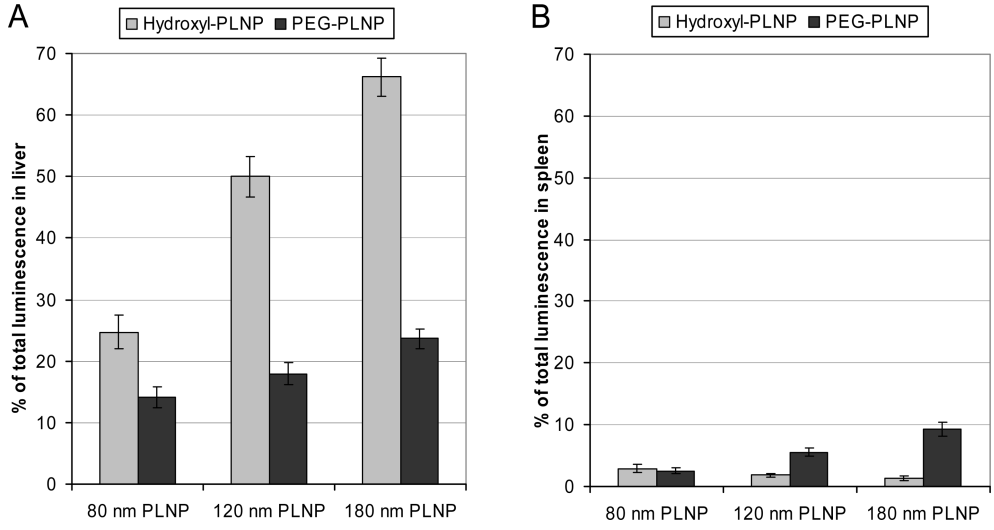

Figure 7. Semiquantitative image-based evaluation of the amount of PLNP located within RES organs, 15 min after the systemic injection in the tail vein (percentage of total luminescence represents the signal from the ROI compared to the one arising from the whole mouse). (A) liver; (B) spleen (n = 6). Error bars correspond to standard deviation.

liver and allowed longer visualization of their probe within the animal.[22] Interestingly, although PEG-covered particles distribute much better through the body, they seem to be directed more likely toward spleen. This tendency, which is particularly noticeable for larger particles, declines with the diameter of the core. Thus, 80 nm PEG-PLNP seem more likely to evade both liver and spleen. These variations can be summarized by calculating the ratio of luminescence in the liver as compared to that in spleen. As shown in Table S2, this ratio, subsequently growing with the hydrodynamic diameter for hydroxyl-PLNP, was stabilized to a much lower value for the PEG-covered PLNP, indicating that stealth PLNP were more likely trapped in spleen.

Unfortunately, luminescence from the smallest particles was hardly distinguishable for periods longer than 15 min after the injection. Therefore, to quantify the PLNP biodistribution after a long period of time, we used an *ex vivo* determination of the delayed fluorescence from europium ions, entrapped in the crystal.

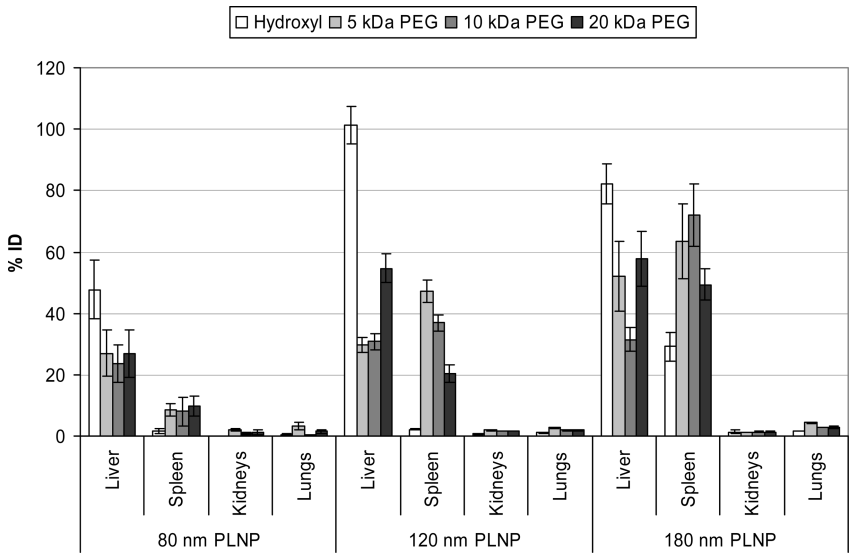

Figure 8. PLNP tissue distribution 6 h after systemic injection to healthy mice (n = 6). Error bars correspond to standard deviation.

***Ex Vivo* Quantitative Biodistribution in Healthy Mice.** Relative long-term biodistribution in healthy mice was achieved 6 h after systemic injection to validate a potential use of this probe for *in vivo* applications. Delayed fluorescence from europium ions allowed an *ex vivo* quantitative analysis through tissue homogenates after animal sacrifice. As shown in Figure 8, similarly to several classes of nanoparticles, and regardless of surface coverage, long-term PLNP biodistribution occurs predominantly within liver and spleen.[23] Combined uptake in the kidneys and lungs remains below 5% of the injected dose. PEG chain length seems to have little influence on the global RES accumulation (combined uptake in liver and spleen), being responsible for a slight change in the liver/spleen ratio (only noticeable for 120 nm PLNP). On the contrary, core diameter appears to be critical. As shown in Supporting Informationi, Table S3, decreasing the particle core diameter from 180 to 80 nm causes a much lower combined RES uptake of PEG-PLNP from 100% down to around 35% of the injected dose. The correlation between particle size and RES accumulation (liver and spleen) 6 h after i.v. injection follows a very similar trend to that observed by semiquantitative analysis 15 min after PLNP administration.

To validate this ability of smaller PEGylated nanoparticles to escape RES uptake, and to assess their propensity to circulate within the body, novel experiments were conducted for which blood was collected by cardiac puncture. As PEG chain length has only poor influence on the combined uptakes within RES organs, we selected the 10 kDa PEG-grafted nanoparticles for this experiment. Indeed, for smallest particles, up to 12.6 $\pm$ 0.8% of the injected dose were retrieved in the blood, indicating that 80 nm PEG-PLNP were still circulating 6 h after the administration. This value is particularly high for nanoparticles of this size and represents approximately three times the percentage retrieved in the blood for 12 nm PEGylated QDs.[24] The amount of material in the blood quickly decreased when increasing the core diameter, down to 3.3 $\pm$ 0.5% for 120 nm PLNP, and to 1.2 $\pm$ 0.1% of the injected dose for 180 PLNP. Our results can be compared to those obtained by Lipka *et al.* with smaller (5 nm inorganic core diameter) radioactive-labeled gold nanoparticles (Au-NPs). They managed to increase, in a significant manner, the circulation time of their Au-NPs after functionalization with PEG 10 kDa and reported that 18% of the injected dose were still circulating 24 h after intravenous injection.[25]

Decreasing nanoparticle size limits RES uptake and allows sustained PLNP blood circulation, thus making them suitable for prospective applications in active targeting. Availability of 10 kDa PEG-covered PLNP, defined as the amount of PLNP in the blood compared to that in harvested organs (see Figure 9A), can be quantified by validating a dimensionless parameter. It is almost increased by a factor of 33 when switching from 180 nm PLNP to 80 nm PLNP.

Spleen/liver ratios, estimated from semiquantitative and quantitative biodistributions of PEGylated PLNP at 15 min and 6 h, are compared in Figure 9B. The relative uptake in spleen and liver is the lowest for 80 nm PLNP, and only slightly increases after 6 h, suggesting that nanoparticles evade the spleen and that distribution remains unmodified after relative long circulation. On the contrary, for 120 and 180 nm PLNP, the ratio switches from a value lower than 1 to one higher, emphasizing a greater accumulation in spleen than in liver, and a highly time-dependent distribution, characteristic of larger PLNP. Schipper *et al.*[26] have already observed a similar trend for smaller particles made of polymer- or peptide-coated ^{64}Cu-labeled QDs to be more likely trapped in spleen after 2 kDa PEG grafting. They showed that PEG functionalization has not only the ability to slow down the

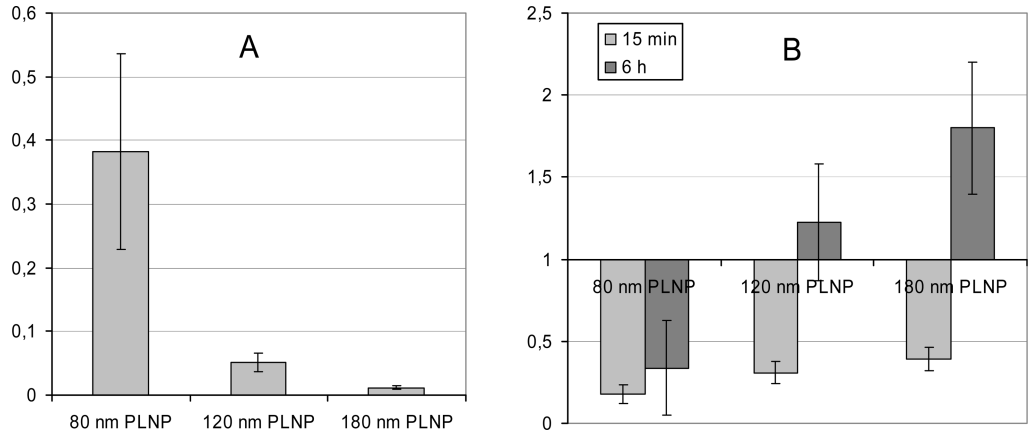

Figure 9. (A) Evolution of the rate (% ID in the blood/cumulated % ID in harvested organs) as a function of the particle core diameter for 10 kDa PEG-covered PLNP (6 h after injection). (B) Evolution of the rate (% ID in the spleen/% ID in the liver) as a function of the particle core diameter at 15 min and 6 h for PEGylated PLNP. Error bars correspond to standard deviation.

uptake process by liver and spleen, but that it can also significantly increase the uptake of nanoparticles by spleen.

***Ex Vivo* Quantitative Biodistribution in Tumor-Bearing Mice.** We finally examined the ability of the long circulating PLNP (80 nm, 10 kDa PEG-covered) to passively target the tumor microenvironment on subcutaneous 3LL tumor-bearing mice. Delayed fluorescence from europium ions allowed quantitative analysis through tumor tissue homogenates after animal sacrifice. Measurements indicate that a non-negligible amount of PLNP ($5.9 \pm 2.8\%$ of the injected dose, $n = 3$) was still located within the tumor microenvironment 6 h after systemic injection. This result, yet certainly due to the fact that 3LL tumor is highly vascularized, is promising for the development of targeted PLNP.

CONCLUSION

We have managed to dramatically extend PLNP circulation in mice by showing that blood retention was highly dependent on the particle core diameter and surface coating. The PEG coverage allowed the formation of stealth particles that globally distributed much better through the animal. However, in opposition to studies reporting the influence of PEG chain length on the biodistribution of small probes,[11] we observed that increasing the molecular weight of the PEG moiety from 5 to 20 kDa had no significant effect on combined uptakes in major RES organs such as liver and spleen.

We also demonstrated that persistent luminescence could be used as a powerful tool for real-time monitoring and semiquantization, in a noninvasive manner. Unfortunately, the long-lasting afterglow remains far too low, preventing access to long-term exploration. Improving PLNP composition could open alternative to new materials with higher quantum yield and brighter luminescence that would allow quantification as well as noninvasive long-term optical imaging.[27]

EXPERIMENTAL SECTION

Chemicals. BOP reagent (benzotriazole-1-yl-oxy-tris-pyrrolidino-phosphonium hexafluorophosphate) was purchased from Advanced ChemTech. (3-Aminopropyl)-triethoxysilane (99%) was obtained from Sigma-Aldrich. Triethylamine (>99.5%) and dimethylformamide (>99.9%) were purchased from SDS. Alpha-methoxy-omega-carboxylic acid poly(ethylene glycol) PEG MW 10.000 and 20.000 Da were bought from Iris Biotech GmbH. The 5.000 Da PEG was previously synthesized from a published protocol of our team.[28]

PLNP Synthesis and Size Selection. Crude and crystallized material was synthesized according to a previously described protocol based on a sol−gel approach[11] followed by a heating at 1050 °C. Nanometer-sized particles were obtained by basic wet grinding of the solid (500 mg) for 15 min with a mortar and pestle in a minimum volume of 5 mM NaOH solution. Hydroxylation was then performed overnight by dispersing the ground powder in 50 mL of the same NaOH solution to get hydroxyl-PLNP.

Nanoparticles with a diameter of 180 nm were selected from the whole polydisperse colloidal suspension by centrifugation on a SANYO MSE Mistral 1000 at 4500 rpm for 5 min (centrifugation time was lengthened to 30 min in order to obtain 120 nm PLNP). They were located in the supernatant (assessed by dynamic light scattering). The supernatants were gathered and concentrated to a final 5 mg/mL suspension. Nanoparticles with a diameter of 80 nm were selected from the 120 nm concentrated suspension by centrifugation on an Eppendorf MiniSpin Plus at 8000 rpm for 5 min. Following the same approach, the centrifugation step was repeated four times and the resulting suspension concentrated to a final amount of 5 mg/mL.

PLNP Functionalization. Nanoparticles were coated according to slightly modified existing protocols.[11] Amino-PLNP were obtained by the addition of 20 μL of 3-aminopropyl-triethoxysilane (APTES) to a suspension of 5 mg of hydroxyl-PLNP in 2 mL of DMF (Scheme 1). The reaction mixture was sonicated the first 15 min using a Branson Ultrasonic Cleaner 1210 and kept under vigorous stirring for 5 h. Particles were washed from the unreacted APTES by three centrifugation and redispersion steps in DMF.

PEG_x-PLNP were obtained by adding 10 μmol of MeO-PEG_x-COOH (50 mg of MeO-$PEG_{5,000}$-COOH, 100 mg of MeO-$PEG_{10,000}$-COOH, and 200 mg of MeO-$PEG_{20,000}$-COOH), 5 mg of BOP reagent, and 5 μL of triethylamine to a suspension of 5 mg of amino-PLNP in 1 mL of DMF (Scheme 1). To ensure a maximum PEG density for all distributions, the last functionalization step was achieved overnight, under vigorous stirring, with a large excess of PEG and BOP

reagent (20-fold molar excess compared to the free amino groups on the surface of amino-PLNP).

Each type of nanoparticles was characterized using transmission electron microscopy (TEM, JEOL JEM-100S), dynamic light scattering, and zeta potential measurements in 20 mM NaCl, performed on a Zetasizer Nano ZS (Malvern Instruments, Southborough, MA) equipped with a 632.8 nm helium neon laser and 5 mW power, with a detection angle at 173° (noninvasive back scattering).

Thermogravimetric analysis (TGA) was performed using a Setaram Setsys evolution 1600 (argon atmosphere; temperature range from 20 to 780 °C, 10 °C/min) on 10 mg dry samples of 120 nm core PLNP, at each functionalization step.

Biodistribution in Healthy Mice. Five weeks old female BALB/c mice (Janvier, Le Genest St. Isle, France) were anesthetized by i.p. injection of a mix of ketamine (85.8 mg/kg) (Centravet, Plancoët, France) and xylazine (3.1 mg/kg) (Bayer, Leverkusen, Germany) diluted in 150 mM NaCl. A 100 μL portion of a colloidal solution (1 mg PLNP resuspended in 1 mL of sterile 150 mM NaCl) was injected in the tail vein. Six hours after the injection, mice were anesthetized, and the blood was collected by cardiac puncture. For extraction of PLNP from the blood, red cells lysis was performed by mixing the specimen with a 5x cell culture lysis reagent from Promega. Hemoglobin was then removed by a series of centrifugation and PLNP were redispersed in 10 mM PBS. Right after cardiac puncture, mice were euthanized by cervical dislocation, and the different organs (liver, spleen, kidney, and lungs) were harvested, weighed, and crushed in 10 mM PBS (5 mL/g tissue). The amount of nanoparticles in a sample was evaluated by measuring delayed fluorescence from europium ions (rare earth doping cations, trapped in the core of our material) using a Wallac Victor^2 Multilabel Counter from Perkin-Elmer (excitation filter, D340; emission filter, D615; counting delay, 1000 μs; counting window, 5000 μs; counting cycle, 6100 μs). Results are given as percentage of the injected dose (% ID).

Biodistribution in Tumor-Bearing Mice. 3LL tumors fragments (about 3 mm^3) were implanted s.c. in both flanks of 5-week-old female C57BL/6 mice (Janvier, Le Genest St. Isle, France), and 15 days later, tumors were harvested for quantization (see method described in previous section for tissue quantization).

Imaging Study. Nanoparticles (1 mg/mL) were excited for 5 min under UV light (254 nm) and injected *via* the tail vein. Immediately after the injection, the animal was placed on its back under the photon-counting device, and the acquisition was performed during 15 min. Signal acquisition was done using a photon-counting system based on a cooled GaAs intensified charge-coupled device (ICCD) camera (Photon-Imager; Biospace, Paris, France) without external excitation source. Acquired images processing, ROI drawing, and semi-quantization were achieved through the use of Biospace developed software, PhotoVision+. Experiments were conducted following the NIH recommendations and in agreement with a regional ethic committee for animal experimentation.

Acknowledgment. This work has been supported by the French National Agency (ANR) in the frame of its program in Nanosciences and Nanotechnologies (NATLURIM project No. ANR-08-NANO-025).

Supporting Information Available: Informations concerning the hydrodynamic diameter of the different PLNP as well as data on the biodistributions. This material is available free of charge *via* the Internet at http://pubs.acs.org.

REFERENCES AND NOTES

1. Weissleder, R.; Pittet, M. J. Imaging in the Era of Molecular Oncology. *Nature* **2008,** *452*, 580–589.
2. Medintz, I. L.; Uyeda, H. T.; Goldman, E. R.; Mattoussi, H. Quantum Dot Bioconjugates for Imaging, Labelling and Sensing. *Nat. Mater.* **2005,** *4*, 435–446.
3. Smith, A. M.; Duan, H.; Mohs, A. M.; Nie, S. Bioconjugated Quantum Dots for *in Vivo* Molecular and Cellular Imaging. *Adv. Drug. Deliver. Rev.* **2008,** *60*, 1226–1240.
4. Li, Z. F.; Ruckenstein, E. Water-Soluble Poly(acrylic acid) Grafted Luminescent Silicon Nanoparticles and Their Use as Fluorescent Biological Staining Labels. *Nano Lett.* **2004,** *4*, 1463–1467.
5. Salonen, J.; Kaukonen, A. M.; Hirvonen, J.; Lehto, V.-P. Mesoporous Silicon in Drug Delivery Applications. *J. Pharm. Sci.* **2007,** *97*, 632–653.
6. Chen, W.; Mahmood, U.; Weissleder, R.; Tung, C. Arthritis Imaging Using a Near-Infrared Fluorescence Folate-Targeted Probe. *Arthritis Res. Ther.* **2005,** *7*, R310–317.
7. Choi, H. S. Renal Clearance of Quantum Dots. *Nat. Biotechnol.* **2007,** *25*, 1165–1170.
8. Longmire, M.; Choyke, P. L.; Kobayashi, H. Clearance Properties of Nano-Sized Particles and Molecules as Imaging Agents: Considerations and Caveats. *Nanomedicine U.K.* **2008,** *3*, 703–717.
9. Park, J. H.; Gu, L.; von Maltzahn, G.; Ruoslahti, E.; Bhatia, S. N.; Sailor, M. J. Biodegradable Luminescent Porous Silicon Nanoparticles for *in Vivo* Applications. *Nat. Mater.* **2009,** *8*, 331–336.
10. Resch-genger, U.; Grabolle, M.; Cavaliere-Jaricot, S.; Nitschke, R.; Nann, T. Quantum Dots *versus* Organic Dyes as Fluorescent Labels. *Nat. Methods* **2008,** *5*, 763–775.
11. le Masne de Chermont, Q.; Chanéac, C.; Seguin, J.; Pelle, F.; Maîtrejean, S.; Jolivet, J.-P.; Gourier, D.; Bessodes, M.; Scherman, D. Nanoprobes with Near-Infrared Persistent Luminescence for *in Vivo* Imaging. *Proc. Natl. Acad. Sci. U. S.A.* **2007,** *104*, 9266–9271.
12. le Masne de Chermont, Q.; Richard, C.; Seguin, J.; Chanéac, C.; Bessodes, M.; Scherman, D. Silicates Doped with Luminescent Ions: Useful Tools for Optical Imaging Applications. *Proc. SPIE* **2009,** *7189*, 71890B/1–71890B/9.
13. Daou, T. J.; Li, L.; Reiss, P.; Josserand, V.; Texier, I. Effect of Poly(ethylene glycol) Length on the *in Vivo* Behavior of Coated Quantum Dots. *Langmuir* **2009,** *25*, 3040–3044.
14. Kim, J.; Seidler, P.; Wan, L. S.; Fill, C. Formation, Structure, and Reactivity of Amino-Terminated Organic Films on Silicon Substrates. *J. Colloid Interface Sci.* **2009,** *329*, 114–119.
15. Sperling, R. A.; Liedl, T.; Duhr, S.; Kudera, S.; Zanella, M.; Lin, C.-A. J.; Chang, W. H.; Braun, D.; Parak, W. J. Size Determination of (Bio)conjugated Water-Soluble Colloidal Nanoparticles: A Comparison of Different Techniques. *J. Phys. Chem. C* **2007,** *111*, 11552–11559.
16. Fang, C.; Shi, B.; Pei, Y.; Hong, M. H.; Wu, J.; Chen, H. Z. *In Vivo* Tumor Targeting of Tumor Necrosis Factor-α-Loaded Stealth Nanoparticles: Effect of MePEG Molecular Weight and Particle Size. *Eur. J. Pharm. Sci.* **2006,** *27*, 27–36.
17. Lecointre, A.; Viana, B.; Le Masne, Q.; Bessière, A.; Chanéac, C.; Gourier, D. Red Long-Lasting Luminescence in Clinoenstatite. *J. Lumin.* **2009,** *129*, 1527–1530.
18. Holsa, J.; Aitasalo, T.; Jungner, H.; Lastusaari, M.; Niittykoski, J.; Giorgio, S. Role of Defect States in Persistent Luminescence Materials. *J. Alloy. Compd.* **2004,** *374*, 56–59.
19. Kudrawiec, R.; Nyk, M.; Syperek, M.; Podhorodecki, A.; Misiewicz, J. Photoluminescence from GaN Nanopowder: The Size Effect Associated with Surface-to-Volume Ratio. *Appl. Phys. Lett.* **2006,** *88*, 181916–181916.
20. Abrams, B. L.; Holloway, P. H. Role of the Surface in Luminescent Processes. *Chem. Rev.* **2004,** *104*, 5783–5801.
21. Kumar, R.; Roy, I.; Ohulchanskky, T. Y.; Vathy, L. A.; Bergey, E. J.; Sajjad, M.; Prasad, P. N. *In Vivo* Biodistribution and Clearance Studies Using Multimodal Organically Modified Silica Nanoparticles. *ACS Nano* **2010,** *4*, 699–704.
22. Ballou, B.; Lagerholm, B. C.; Ernst, L. A.; Bruchez, M. P.; Waggoner, A. S. Noninvasive Imaging of Quantum Dots in Mice. *Bioconjugate Chem.* **2004,** *15*, 79–86.
23. Minchin, R. F.; Martin, D. J. Nanoparticles for Molecular Imaging—An Overview. *Endocrinology* **2010,** *151*, 474–481.
24. Schipper, M. L.; Cheng, Z.; Lee, S.; Bentolila, L. A.; Iyer, G.; Rao, J.; Chen, X.; Wu, A. M.; Weiss, S.; Gambhir, S. S. MicroPET-based Biodistribution of Quantum Dots in Living Mice. *J. Nucl. Med.* **2007,** *48*, 1511–1518.
25. Lipka, J.; Semmler-Behnke, M.; Sperling, R. A.; Wenk, A.; Takenaka, S.; Schleh, C.; Kissel, T.; Parak, W. J.; Kreyling,

W. G. Biodistribution of PEG-Modified Gold Nanoparticles Following Intratracheal Instillation and Intravenous Injection. *Biomaterials* **2010,** *31*, 6574–6581.
26. Schipper, M. L.; Iyer, G.; Koh, A. L.; Cheng, Z.; Ebenstein, Y.; Aharoni, A.; Keren, S.; Bentolila, L. A.; Li, J.; Rao, J.; Chen, X.; Banin, U.; Wu, A. M.; Sinclair, R.; Weiss, S.; Gambhir, S. S. Particle Size, Surface Coating, and PEGylation Influence the Biodistribution of Quantum Dots in Living Mice. *Small* **2009,** *5*, 126–134.
27. Van den Eeckhout, K.; Smet, P. F.; Poelman, D. Persistent Luminescence in Eu^{2+}-Doped Compounds: A Review. *Materials* **2010,** *3*, 2536–2566.
28. Masson, C.; Scherman, D.; Bessodes, M. 2,2,6,6-Tetramethyl-1-piperidinyl-oxyl/[bis(acetoxy)-iodo]benzene-mediated Oxidation: A Versatile and Convenient Route to Poly(ethylene glycol) Aldehyde or Carboxylic Acid Derivatives. *J. Polym. Sci., A1* **2001,** *39*, 4022–4024.